Available online at www.sciencedirect.com
SCIENCE DIRECT®
C. R. Physique 5 (2004) 857–879
COMPTES RENDUS PHYSIQUE
http://france.elsevier.com/direct/COMREN/

Fundamental metrology/Métrologie fondamentale

Fundamental electrical standards and the quantum metrological triangle

François Piquemal *, Alexandre Bounouh, Laurent Devoille, Nicolas Feltin, Olivier Thevenot, Gérard Trapon

BNM-LNE, 29, avenue Roger-Hennequin, 78197 Trappes cedex, France

Available online 6 November 2004

Presented by Guy Laval

Abstract

The advent of the fundamental constants R_K (the von Klitzing constant) and K_J (the Josephson constant) in electrical metrology and the growing development of nanotechnologies have totally changed the vision and the practice of the National Metrology Institutes (NMIs), opening a modern era of metrology and arousing a growing interest in a possible re-definition of the international system of units (SI). The Josephson effect (JE) and the Quantum Hall effect (QHE), at the origin of these fundamental constants, constitute the keystone of a new approach to electrical units, when one considers the very high level of reproducibility of these units, never seen before. On the other hand, the Watt balance experiment in which these constants play a part could be the origin of a new SI definition, replacing the mass unit 'the kilogram' as a fundamental unit by the Planck constant h. It thus seems that the implementation of experiments aimed at demonstrating the coherency between the theoretical and phenomenological values of these constants is a major objective. In this framework the metrological triangle experiment associating QHE, JE and single electron tunnelling effect would play a major role in checking the consistency of these fundamental constants in terms of the Planck and electron charge constants. This article gives briefly an outline of these quantum phenomena and their metrological applications in NMIs for the realisation of electrical units and the determination of the fundamental constants. ***To cite this article: F. Piquemal et al., C. R. Physique 5 (2004).***

Résumé

Étalons électriques fondamentaux et le triangle métrologique quantique. L'avènement des constantes fondamentales R_K (von Klitzing) et K_J (Josephson) dans la métrologie électrique et le développement considérable des nanotechnologies ont totalement bouleversé la vision et la pratique des Laboratoires Nationaux de Métrologie (LNMs) ouvrant ainsi une ère nouvelle, incontestablement moderne de la métrologie et suscitant un intérêt croissant pour une possible re-fondation du système international d'unités (SI). L'effet Josephson (EJ) et l'effet Hall quantique (EHQ), à l'origine de ces constantes fondamentales, constituent la clé de voûte d'une nouvelle approche des unités électriques compte tenu du très haut niveau de reproductibilité de ces unités jamais atteint auparavant. D'autre part, une expérience comme la balance du watt dans laquelle ces constantes interviennent pourrait être à l'origine d'une nouvelle définition du SI dans lequel la constante de Planck h prendrait le pas sur l'unité de masse « le kilogramme ». Il apparaît donc que la mise en œuvre d'expériences visant à démontrer la cohérence entre les valeurs théoriques et phénoménologiques de ces constantes soit un objectif majeur. C'est dans ce cadre qu'intervient l'expérience du triangle métrologique par l'association de l'EHQ, l'EJ et l'effet tunnel à un électron pour vérifier la cohérence

* Corresponding author.
E-mail address: francois.piquemal@lne.fr (F. Piquemal).

1631-0705/$ – see front matter
doi:10.1016/j.crhy.2004.08.006

de ces constantes fondamentales en terme des constantes de Planck et de charge de l'électron. Cet article donne brièvement un aperçu de ces phénomènes quantiques et leurs applications métrologiques dans les LNMs pour la réalisation des unités électriques et la détermination des constantes fondamentales. ***Pour citer cet article : F. Piquemal et al., C. R. Physique 5 (2004).***

Keywords: Fundamental electrical standards; International system of units; Fundamental constants; Josephson effect; Quantum Hall effect; Single electron tunnelling; Quantum metrological triangle

Mots-clés : Étalons électriques fondamentaux ; Système international d'unités SI ; Constantes fondamentales ; Effet Josephson ; Effet Hall quantique ; Effet tunnel à un électron ; Triangle métrologique quantique

1. Introduction

In the present SI system, the base units, metre, kilogram and second, allow one to define derivative units such as the newton, joule, watt, but also the fourth base unit, the ampere, from which all electrical units are defined [1]. In theory, the link between electrical and mechanical units is made through an SI realisation of the ampere. However, in practice, it is more relevant to realise first the derivative electrical units, farad and ohm on the one hand, volt in the other (Fig. 1). This allows the determination of the ampere afterwards with a higher accuracy. The farad undoubtedly occupies the first place in the hierarchy of electrical units. Its definition in the SI system and its reproducibility are possible by means of a Thompson–Lampard calculable capacitor [2]. In addition, the setting-up of the calculable capacitor makes possible the SI realisation of the ohm through a comparison between the impedances of capacitor and resistor. This leads to a determination of the von Klitzing constant R_K originating from the quantum Hall effect (QHE) [3–8]. This effect links a resistance to a fundamental constant, just as the ac Josephson effect (JE) [9–13] links electromotive force to another fundamental constant, the Josephson constant K_J. Furthermore, theory predicts that $R_K = h/e^2$ and $K_J = 2e/h$.

These two phenomena have a great impact in metrology because, firstly, they provide fundamental standards with values independent of space and time, setting uniquely the representation of the ohm and the volt over the world. Secondly, through the SI realisation of electrical units, QHE and JE contribute significantly to the improvement of the knowledge of constants of nature [14,15]. For instance, the SI realisations of the ohm and the *electrical* watt (as proposed by the moving-coil Watt balance experiments [16]) lead to the determination of the well-known fine structure constant $\alpha = \mu_0 c/(2h/e^2)$ and the Planck constant, if one assumes that QHE and JE give h/e^2 and $2e/h$ exactly.

Following the examples of QHE and JE, a third quantum phenomenon, the single electron tunnelling (SET) effect [17,18], has applications which can disrupt again electrical metrology. In practice, the ampere is reproduced by means of the ohm and the volt, but the direct use of SET becomes relevant when the amplitude of the current is less than 1 nA. This phenomenon

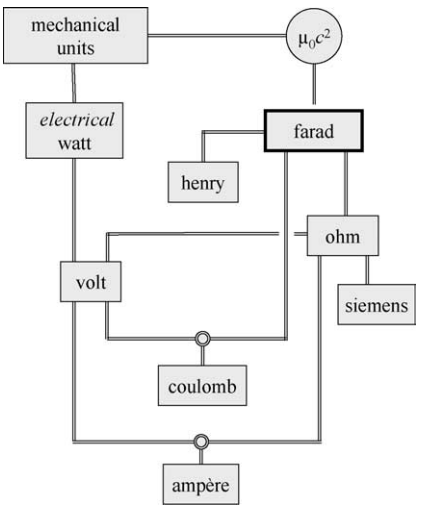

Fig. 1. Chain of SI realisations of electrical units. According to the definition of the ampere, the value of the permeability of vacuum μ_0 is fixed: $\mu_0 = 4\pi \times 10^{-7}$ N/A^2.

indeed makes possible the development of a quantum standard of current whose amplitude is directly linked to the electron charge. From a 'classical' point of view, SET would restore the ampere and the coulomb in the foreground. More important is the experimental possibility of testing directly the coherence of the constants involved in QHE, JE and SET phenomena which are robustly alleged to provide the free space values of h/e^2, $2e/h$ and e. This is the task of the quantum metrological triangle experiments from Likharev and Zorin's proposal [19]. These experiments consist either in applying Ohm's law $U = RI$ [20], or in following $Q = CU$ from the realisation of an electron counting capacitance standard. From a 'modern' point of view, the closure of the quantum metrological triangle at a level of one part in 10^8 will establish *a bridge between microscopic and macroscopic physics* [21], and will play an important role toward the foundation of a new SI system fully based on fundamental constants.

The paper is structured respecting the present-day practical chain of electrical units and starts by a description of the Thompson–Lampard calculable capacitor. Sections 3 and 4 deal with the quantum standards of resistance and voltage respectively. The theory of SET and devices are outlined in Section 5 and then the metrological triangle experiments are explained in Section 6. Conclusions and prospects are given in Section 7.

2. Thompson–Lampard calculable capacitor

The farad is presently the electrical unit that is realised in SI units with the smallest uncertainty. This result comes from a 'mise en pratique' of the theorem discovered by Thompson and Lampard in 1956 [2] and gave rise to a calculable capacitance. This theorem stipulates that for a cylindrical system (Fig. 2) composed of four isolated electrodes of infinite length placed in vacuum, the direct capacitances per unit of length γ_{13} and γ_{24} of two pairs of electrodes obey the relation:

$$\exp(-\pi\gamma_{13}/\varepsilon_0) + \exp(-\pi\gamma_{24}/\varepsilon_0) = 1, \tag{1}$$

where ε_0 is the permittivity of vacuum. Moreover, in the case of a perfect symmetry with identical capacitances per unit of length, it results:

$$\gamma_{13} = \gamma_{24} = \gamma = (\varepsilon_0 \ln 2)/\pi = 1.953549043\ldots \text{ pF/m}$$

and then a value of the electrical capacitance can be directly linked to a length measurement.

From the outstanding work of Clothier at NMI (formerly CSIRO/NML) [22], the most accurate implementation of the theorem is to assemble a system of four identical long parallel and slightly spaced cylindrical electrodes (bars), placed vertically at each corner of a square. A movable grounded bar is placed in the cross section of the four main bars. In practice, to avoid end effects, the measurements are carried out by comparing a fixed capacitance to the capacitance variation of the calculable capacitor for two positions of the movable bar. The length of this displacement is measured by means of a laser interferometer, thus allowing the link of the farad to the metre.

The theorem can be applied to a system composed of more than four electrodes. Thus the BNM calculable capacitor consists of five electrodes in the horizontal position arranged at the vertices of a regular pentagon [23,24]. This unique feature strongly differs from the calculable capacitors developed by the other NMIs (NIM, NIST, NMI, NPL, PTB). If one connects successively two of the adjacent bars, a five-bar system is equivalent to five different four-bar systems in turn and the theorem can be applied to each of these five systems. In the ideal case of perfect symmetry, the capacitance per unit of length between two non-adjacent bars is equal to 2γ such that:

$$\exp(-2\pi\gamma/\varepsilon_0) + \exp(-\pi\gamma/\varepsilon_0) = 1 \tag{2}$$

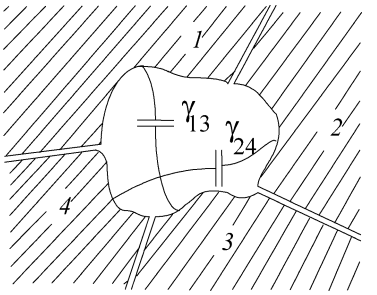

Fig. 2. Cross section of a structure with four electrodes. γ_{13} and γ_{24} are capacitances by unit of length.

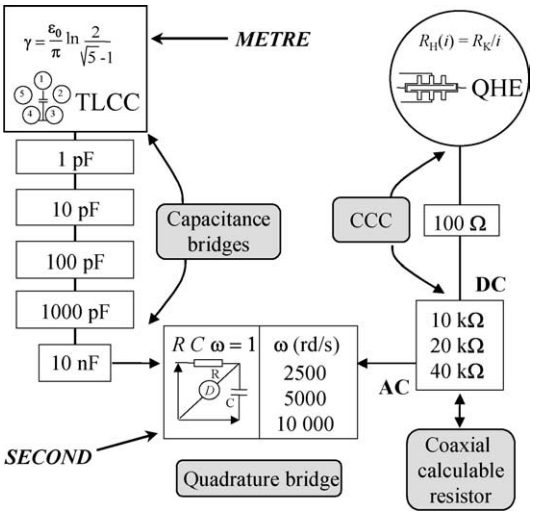

Fig. 3. Measurement method employed at BNM-LNE to determine R_K in SI units from a Thompson–Lampard calculable capacitor (TLCC) [24]. The measurements are carried out at three frequencies in order to take into account the frequency dependence of the TLCC itself.

leading to:

$$\gamma = (\varepsilon_0/\pi)\ln\left[2/(\sqrt{5}-1)\right] \text{ F/m} = 1.356235626\ldots \text{ pF/m}.$$

The main difficulties to overcome for elaborating any calculable capacitor lie in the alignment of all electrodes, the movable guard and its trajectory. Moreover, the section of the cylindrical electrodes has to be as regular as possible. Fitting the end of the movable guard with a spike is the usual method for significantly reducing the residual cylindricality defect in the cross section of the capacitor [22]. Another error source arises from the frequency effect, which can be due, for example, to the self-inductance of the electrodes [22] or to electrical connections [24]. The highest accurate calculable capacitors allow a SI value of the farad with an uncertainty of a few parts in 10^8.

By means of a complete measurement chain, the calculable capacitors have made possible SI realisations of the ohm and then of R_K. The keystone of the set up is a quadrature bridge, which allows one to compare, with a very high accuracy, impedances of two resistances R_1 and R_2 against two capacitances C_1 and C_2 first linked to the calculable capacitor. The bridge is balanced when the equation $R_1R_2C_1C_2\omega^2 = 1$ is true, ω being the pulsation of the applied voltages. In practice, C_1 and C_2 have nominal values ranging from 1 nF to 10 nF. They are compared to the calculable capacitor by successive measurements of capacitance ratios involving transfer standards of 1 pF, 10 pF and 100 pF. The nominal values of R_1 and R_2 are contained between 10 kΩ and 100 kΩ and ω is about 10 000 rad/s typically. After correction of their frequency variations by means of an ac-dc calculable resistor [24], these resistances are also compared in DC to the QHR, giving a SI value of R_K. DC measurements are carried out by means of a CCC resistance bridge (described in next section). The overall view of the successive measurements at BNM is shown on Fig. 3.

The best SI realisations of the ohm and thus of R_K have uncertainties between 2 and 6 parts in 10^8 [15,23]. Fig. 4 shows the weighted mean values of α^{-1} determined through R_K and by indirect methods (anomalous magnetic moment of electron, quotient of Planck constant and either relative atomic mass of cesium or neutron mass times lattice spacing of a crystal, shielded gyromagnetic ratio of proton in high field, ground state hyperfine transition frequency of muonium). All measurements agree within a range of ± 1 part in 10^7, hence the decision of CIPM to reduce the uncertainty of R_K from 2 parts to 1 part in 10^7 [25], while keeping the conventionally true value $R_{K\text{-}90} = 25\,812.807\ \Omega$ for metrological purpose [1,26]. Furthermore, the 2002 adjustment of fundamental constants performed by the CODATA group [15] leads to values of $\alpha^{-1} = 137.03599911$ and $R_K = R_{K\text{-}90}(1 + 1.74 \times 10^{-8})$ with the same standard deviation uncertainty of 3.3 parts in 10^9 [15].

The required efforts for realising calculable capacitors have forced some NMIs to give up their work and to move towards maintaining the farad from the QHE. However, as reported below, the aim in reducing the uncertainty on R_K value in SI units down to one part in 10^8 is a strong motivation for some NMIs such as NMI and BNM-LNE to pursue their efforts in improving calculable capacitors and for other laboratories, as BIPM, to start the development of such a standard.

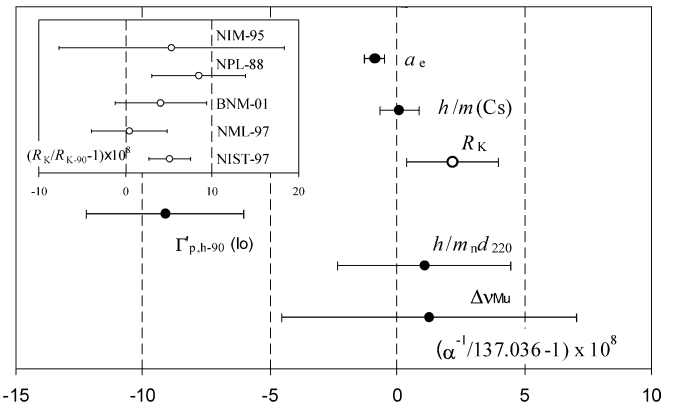

Fig. 4. Mean values of α^{-1} obtained by SI determinations of R_K (in insert), and by indirect methods [15].

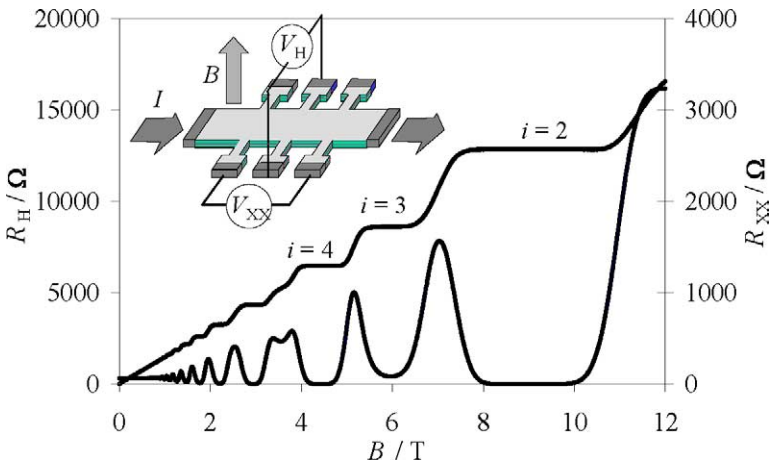

Fig. 5. Quantized Hall resistance (QHR) R_H and longitudinal resistance R_{XX} as a function of B for GaAs/AlGaAs heterostructure at $T = 180$ mK and crossed by a current of 8 μA.

3. Quantized Hall resistance standard

3.1. Integer quantum Hall effect

The quantum Hall effect (QHE) discovered by von Klitzing in 1980 [3] is observed at low temperature and under a high magnetic flux density in a two-dimensional electron gas (2DEG). The Hall resistance of the 2DEG exhibits a set of plateaux centred on quantized values dependent only on the fundamental constant h/e^2:

$$R_H(i) = h/ie^2, \tag{3}$$

where i is an integer. Each plateau of resistance is correlated with an abrupt drop of the longitudinal resistance R_{XX} with minimal values that can be less than 100 μΩ as observed for $i = 2$ or 4 plateaux, usually used (Fig. 5). The 2DEG is created either in the inversion layer at the interface of a silicon MOSFET, or at the junction of semiconductors with different energy band gaps. GaAs/AlGaAs heterostructure is the prime system for metrological applications of QHE. The Hall bar sample as shown in Fig. 6 is realised by lithographic techniques. It consists of an active area delimited by a 300 nm thick mesa with AuGeNi contacts on each of the eight terminal pads.

Laughlin has given a general theoretical explanation of QHE using a topological argument and based on the concept of the mobility gap and the gauge invariance [28]. Büttiker has proposed a formulation based on the edge states where the current is flowing only through the sample edges, emphasizing the role of the contacts acting as reservoirs [29]. However, all these approaches predict the QHE properties at zero temperature and at no dissipation state. Actually, among the variety of the proposed models, no one at the present time is able to take into account, firstly, the real experimental conditions of the non-zero

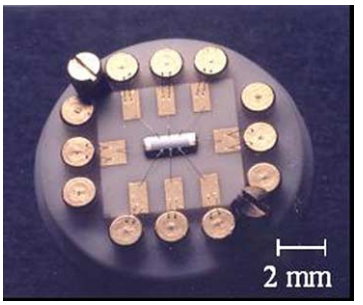

Fig. 6. Hall bar sample of LEP514 type mounted on TO-8 holder [27].

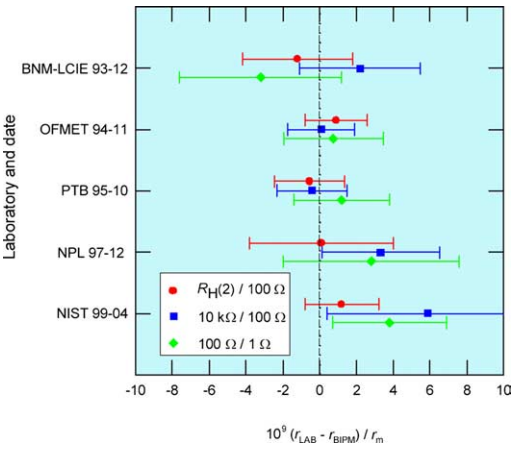

Fig. 7. Results of the bilateral comparisons between BIPM (with transportable QHE system) and BNM-LCIE, OFMET, PTB, NPL and NIST. Error bars mean one standard deviation estimate of combined uncertainty [34].

temperature, the finite magnetic field and the high current value, which lead to a dissipative state, and, secondly, the imperfect nature of the Hall sample and its contacts. Detailed bibliographies on both theoretical and experimental works can be found in references [4–8].

3.1.1. Universality and von Klitzing constant

The quantized Hall resistance (QHR), theoretically linked to h/e^2, might be used as a reference standard of resistance if the QHE sample respects the criteria given by CCEM technical guidelines [30]. Under these conditions, QHE allows one to realise a highly reproducible reference standard. Indeed, measurements have shown values of the product $i \times R_H(i)$ independent of the sample properties (growth techniques, type of structure, technological and geometrical parameters), of the used plateau ($i = 1$, 2, 4, 6 or 8) and of the experimental conditions (temperature, measuring current amplitude) with uncertainties as low as few parts in 10^{10} [31,32].

Moreover, bilateral comparisons of complete QHE systems performed between BIPM and some NMIs during the past decade (Fig. 7) [33] or more recent international comparisons involving 1 Ω or 100 Ω travelling standards, have shown excellent agreement of a few parts in 10^9 [35,36]. These results, which strongly support the universal aspect of the constant involved in QHE, confirm the conclusiveness of the 1988 CIPM recommendation for the use of QHR as a resistance standard. This unique representation of the ohm constitutes a watershed compared with the former situation when national bases were constituted by wire-wounded resistance standards drifting in time, depending on ambient conditions (temperature, pressure), and which materialised only a local value of the ohm.

It is noteworthy that the design requirements make the fabrication of QHE samples for metrological purposes difficult and sources providing these are lacking. Specific projects for producing a large number of QHE samples have been undertaken by NMIs in order to partly solve this problem [27,37,38].

3.2. CCC-based resistance bridge

Most of the resistance bridges currently used in NMIs to calibrate resistances against QHR are based on a cryogenic current comparator (CCC). This is the instrument which has allowed one to demonstrate the universality of R_K with the high accuracy mentioned above. It is briefly described below. More details on CCC can be found in the literature [10,39].

The principle of CCC, invented by Harvey in 1972 [40], rests on Ampère's law and the perfect diamagnetism of a superconductor in the Meissner state. Given two wires inserted in a superconducting tube (Fig. 8), currents I_1 and I_2 circulating through these wires will induce a supercurrent I flowing up the inner surface of the tube and backing down the outer surface in such a way to maintain a null magnetic flux density B inside the tube. Application of Ampère's law to a closed contour (a) in the bulk gives:

$$\oint_a B \cdot \mathrm{d}l = 0 = \mu_0 \cdot (I_1 + I_2 - I) \tag{4}$$

and leads to the equality of the currents:

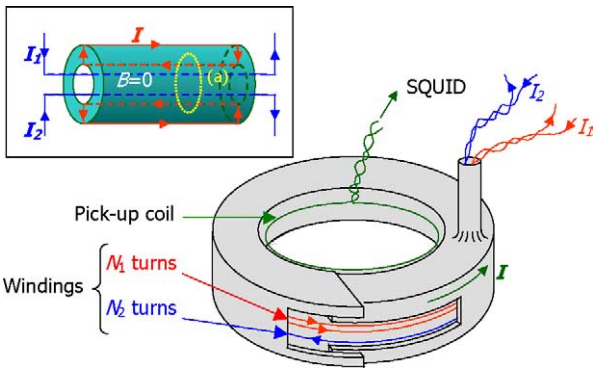

Fig. 8. Toroidal structure of a CCC and principle (in insert). The supercurrent flowing up the inner surface of the toroïdal shield is given by $I = N_1 I_1 + N_2 I_2$.

$$I = I_1 + I_2. \tag{5}$$

If the tube contains N_1 and N_2 wires crossed respectively by currents I_1 and I_2, then (5) becomes:

$$I = N_1 I_1 + N_2 I_2. \tag{6}$$

These equalities are valid independently of the position of the wires inside the tube. Here is the key reason for the high accuracy of the CCC. In practice, a CCC is made of two windings with N_1 and N_2 turns crossed by currents I_1 and I_2 circulating in opposite directions. These windings are enclosed in a superconducting torus [41], whose extremities overlap without being electrically connected on a length large enough to overcome the end effects, which distort the current equality in the real case of a finite length tube (Fig. 8).

The outside magnetic flux, which results only from the supercurrent, is detected by a SQUID and the voltage at the output is then converted in a current which feeds back one of the two windings to null the magnetomotive forces:

$$N_1 I_1 - N_2 I_2 = 0. \tag{7}$$

A CCC connected to a double constant current source [42] which supplies resistances R_1 and R_2 to be compared with I_1 and I_2 is sketched on Fig. 9. The operation consists in deviating a fraction ε of current I_2 in an auxiliary winding of N_a turns in order to balance the bridge both in voltage and in ampere turns. It results in the resistance ratio:

$$R_1/R_2 = N_1/N_2 \cdot \left[1 + (N_a/N_2)\varepsilon\right], \tag{8}$$

where ε is determined by different methods.

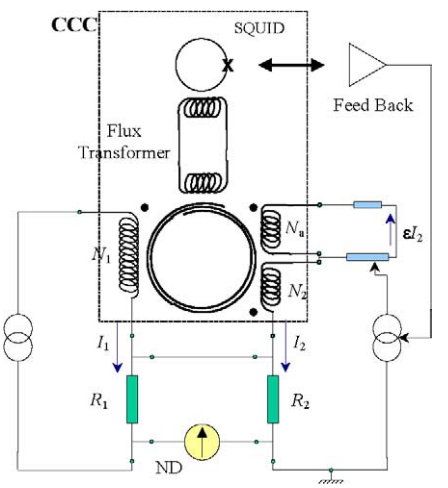

Fig. 9. Circuit diagram for a CCC-based resistance bridge. The fraction ε of the secondary current I_2 is deviated into an auxiliary winding by means of a resistive divider.

3.3. Quantized Hall array resistance standard

The metrological applications of QHE from a single Hall bar are only limited to resistance standards with a nominal value of $R_K/2$ and $R_K/4$, i.e. around 10 kΩ. Plateaux corresponding to odd or high value of i are generally not well quantized. Moreover, the maximum current that can be supplied to single Hall bars does not typically exceed 100 μA. Special resistance bridges, such as based on CCC, whose use is restricted to NMIs, are therefore required to calibrate material resistance standard with QHE. Fortunately, by means of a multiple connections technique with redundant links between QHE samples connected in series or in parallel, new quantum resistance values can be obtained. This technique proposed by Delahaye [43] allows one to cancel the contact resistance effect, and consequently to define the four terminal resistance of the equivalent quantum resistors. Expressing by ε ($\varepsilon \ll 1$) the typical resistance of a contact between two Hall bars relative to the value of R_H, the relative error contribution to the Hall resistance is limited to ε^n, where n is the number of links. This technique uses two fundamental properties of QHE: the two-terminal resistance between any pair of probes and the four-terminal longitudinal resistance are ideally equal to R_H and zero respectively. The metrological proof of the efficiency of the multiple connections technique was first obtained for two Hall bars placed in parallel [33,43], and then for Hall bars connected in auto-series [44]. After realising the first series array of ten Hall bars [44], BNM has developed quantum Hall array resistance standards (QHARS) with nominal values in the wide range $R_K/200$ to $50R_K$ [45–48]. For example, Fig. 10 shows a QHARS, which consists in multiple connected Hall bars in a series-parallel arrangement in such a way that the nominal value is equal to $16 \times R_K/4130$, so very close to 100 Ω [47]. Fig. 11 shows QHE curves obtained from QHARS of 129 Ω and 258 Ω on $i = 2$ plateau. Their resistances have been found equal to their nominal values within an uncertainty of 5 parts in 10^9 with a measuring current as high as 4 mA and at a temperature of 1.3 K. The development of such QHARS, which are real quantum standards, in the image of the successful Josephson array voltage standards, needs to be pursued because they open new prospects on metrological applications of QHE:

(1) The calibration of resistances with nominal values up to 1 MΩ or down to 1 Ω is possible without using transfer standards of intermediate values, and consequently the uncertainties can be reduced by a factor of 10 or 100 (a few parts in 10^7 for 1 MΩ, one part in 10^9 for 1 Ω).
(2) The consistency of the ohm representation in the NMIs might be checked with a very high accuracy and less difficulty by using QHARS as travelling standards in place of resistors (1 Ω or 100 Ω) or instead of moving a complete QHE system [33]. The uncertainties could be reduced at a level not yet reached in the frame of international comparisons of resistances.
(3) QHARS are compatible with conventional bridges typically used in industrial calibration centres and commercially available. For instance, resistance standards can be directly calibrated against QHARS of parallel type, which might tolerate high current such as that supplied by a room temperature current comparator.

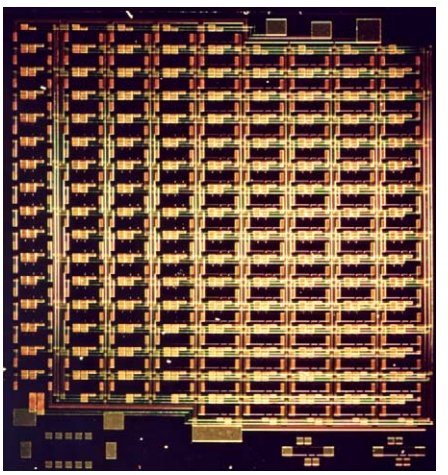

Fig. 10. QHARS of 100 Ω nominal value (square of 10 mm of side) developed at BNM-LNE. The array is composed of a subarray of 129 Hall bars (200 µm thick) placed in parallel by using the triple connections technique and this subarray is connected in parallel with another subarray of 16 bars placed in series [47].

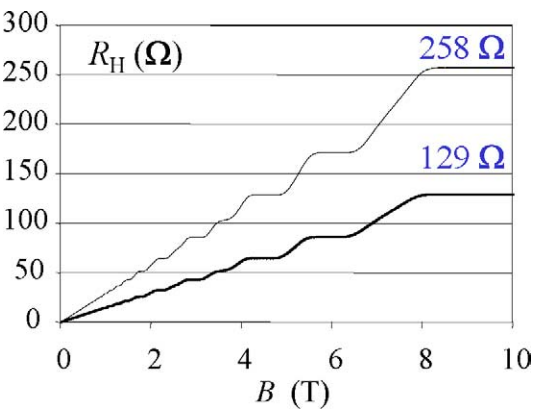

Fig. 11. Dependence of R_H on B for two QHARS, with resistances of 129 Ω and 258 Ω on $i = 2$ plateau [45]. These QHARS are respectively composed of 100 and 50 Hall bars connected in parallel by triple connections.

3.4. AC QHR standard

For more than one decade, NMIs and BIPM have investigated the use of QHR as an impedance standard in the audio frequency range [49]. The aim is to improve the metrological chain linking resistance and capacitance in the framework of the SI realisation of the ohm, and vice versa in the reproducing of the farad from the ohm. So far, the frequency correction of the resistances used in the capacitance–resistance measurement chain needs a comparison against an ac-dc resistor for which the frequency variation is calculable. Variations of less than one part in 10^9 from dc to 1 kHz reported for the best ac-dc resistors can be considered as a requirement for the use of an ac QHR standard in the frame of the determination of R_K.

The ac measurement techniques for QHR have been significantly improved. The main difficulties arose from the fairly resistive cryogenic coaxial cables needed for connecting the QHE sample to the impedance bridge. The adoption of multiple connections technique [43] and the use of active current equalizers [50] in place of passive connectors have been found well suited to reducing the best measurement uncertainties. As a consequence, some controversial results about the frequency effect on QHR have been partly explained. However, the linear dependence of QHR on frequency and current usually measured, which would be correlated to an ac loss mechanism in the QHE device, remains unclear. Indeed, one can reduce this linear variation by different methods either by the use of gated samples or of specific sample holders [49–51]. The frequency coefficient on QHR has thus been obtained within a few parts in 10^8 per kilohertz. Consequently, the calibration of capacitance in terms of ac QHR is possible at an uncertainty level of one part in 10^7 [52]. Further experimental and theoretical investigations are required to conclude if QHE can provide a true quantum impedance standard.

4. Josephson voltage standard

4.1. Josephson effects and universality of K_J

Electrical metrology has entered a quantum era in 1962 when Josephson [8,9] discovered a remarkable consequence of the macroscopic coherence of the superconducting state. The Josephson effects (JE) take place at low temperature in a junction of two weakly coupled superconductors, e.g. two superconducting electrodes separated by a thin insulating layer. In each superconductor, the electrons paired in Cooper pairs form a condensate which is described by a unique wavefunction, $\psi = A\mathrm{e}^{\mathrm{i}\phi}$ with a phase ϕ coherently maintained over macroscopic distances. Josephson predicted two effects:

- Cooper pairs tunnel the junction even at zero voltage drop between the terminals, giving a dc supercurrent $I_J = I_C \sin\phi$, where I_C is a constant and $\phi = \phi_1 - \phi_2$ is the phase difference between the wavefunctions in the two superconductors;
- A constant voltage U through the junction induces an oscillation of the tunnel supercurrent at a frequency $f = (2e/h)U$ ($2e/h$ corresponding to the inverse of the flux quantum Φ_0). It leads to the time variation of the phase due to an energy change $2eU$ involved when a Cooper pair is tunnelling:

$$\mathrm{d}\phi/\mathrm{d}t = (2e/\hbar)U. \tag{9}$$

This second effect, called the ac Josephson effect (JE) and first observed by Shapiro [53], provides a perfectly reproducible and universal voltage standard, since the voltage is directly linked to the frequency.

The craze of metrologists since 1970s for JE as a mean of maintaining the volt results from both theoretical and experimental works, which tend to verify the validity of the relation $f = (2e/h)U$. From topological arguments, Bloch [54] has shown that the constant involved in this relation is $2e/h$ exactly. Numerous experiments have investigated the dependence of the voltage-frequency ratio on materials (Pb, Sn, In, Nb, and more recently YbaCuO) or on junction types (microbridge, tunnel junction or point contact). An upper limit less than 2 parts in 10^{16} has been established so far [55].

From early on, JE has then been used for reproducing the volt. However, because of slightly different values of $2e/h$ obtained from SI realisations of the volt, no international consensus on a single value was possible. Fortunately, a better agreement was found between determinations of $2e/h$ performed in 1980s. This has allowed the CIPM to recommend implementing JE as a voltage standard, using the Josephson constant K_J as an estimate of $2e/h$, and for calibration purpose by assigning to it one single value [56]:

$$K_{J\text{-}90} = 483597.9\ \text{GHz/V exactly}.$$

In terms of SI units, the uncertainty on K_J is 4 parts in 10^7 until now.

4.2. Current–voltage characteristics of a Josephson junction

The dynamic behaviour of a real Josephson junction connected to an external circuit can be described by means of the Resistively and Capacitively Shunted Junction (RCSJ) model proposed by Stewart [57] and Mc Cumber [58]. In this model, the equivalent circuit of the junction consists of three arms in parallel respectively crossed by:

- the supercurrent $I_J = I_C \sin\phi$;
- the current carried by quasi particles (due to broken Cooper pairs since $T \neq 0$), $I_q = U/R$ where U is the voltage drop across junction terminals and R is approximately the tunnel resistance of the junction;
- the displacement current $I_D = C\,\mathrm{d}U/\mathrm{d}t$ through the capacitance C between superconducting electrodes.

The sum of these currents has to be equal to the current I ($I = I_{dc} + I_1 \sin\omega t$) supplied to the junction by the external source. After eliminating U given by relation (9), it results a 2nd order non-linear differential equation:

$$I = (\hbar C/2e)\,\mathrm{d}^2\phi/\mathrm{d}t^2 + \hbar/(2eR)\,\mathrm{d}\phi/\mathrm{d}t + I_C \sin\phi. \tag{10}$$

Introducing dimensionless quantities $i = I/I_C$ and $\tau = 2\pi f_P t$, where $f_P = (\underline{e} I_C/(\pi h C))^{1/2}$ is the plasma frequency, (10) becomes:

$$i = \mathrm{d}^2\phi/\mathrm{d}\tau^2 + \beta_C^{-1/2}\,\mathrm{d}\phi/\mathrm{d}\tau + \sin\phi, \tag{11}$$

where $\beta_C = (2\pi RCf_P)^2$ is the Mc Cumber parameter. In the general case of non-negligible junction capacitance, these equations ((10) or (11)) have to be solved numerically.

For overdamped junctions ($\beta_C \leqslant 1$) supplied with an alternative current at a microwave frequency f, it is found that the I–V characteristic can exhibit a series of stable voltage steps at constant values:

$$U_n = n(h/2e)f \tag{12}$$

with n an integer.

4.3. Josephson array voltage standard (JAVS)

The first Josephson standards were based on single overdamped junctions. They generated only voltage of a few mV (typically operating on high-order steps, $n > 500$, at $f \approx 10$ GHz). The calibration of the former primary standards such as 1.018 V saturated Weston cell then implied the use of a voltage divider and the final uncertainty was limited at a level of 100 nV. Reducing this uncertainty would naturally induce the increase of the Josephson voltage by placing in series a certain number of junctions. Levinson et al. suggested to use underdamped junctions ($\beta_C > 1$) which have the great advantage of delivering several voltage steps at zero bias current if the radiation frequency is much higher than the plasma frequency [59]. Consequently, only a single current source is necessary to bias an array of N junctions placed in series. In the frame of NIST-PTB collaboration, first 1 V voltage arrays made of 2000 to 3000 superconductor–insulator–superconductor (SIS) junctions were elaborated [60]. 1 V and 10 V arrays [61,62], the latter being composed of more than 10 000 junctions, are now commercially available.

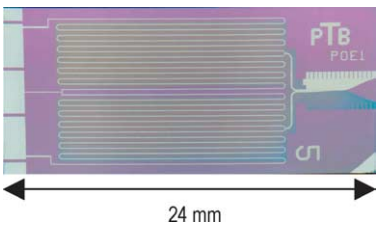

Fig. 12. PTB 10-V array composed of 13 924 junctions ($18 \times 50\ \mu m^2$) in series [62] (photograph by courtesy of the PTB).

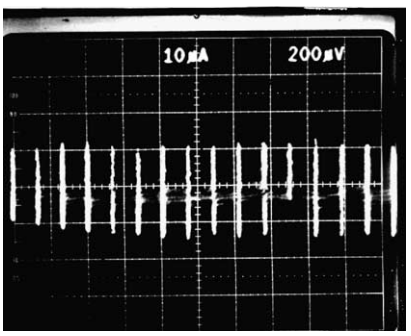

Fig. 13. Voltage steps around 10 V observed on the I–V characteristic of a 10 V array with 80 GHz microwave irradiation.

In addition to the design requirements [63,64] on the junction parameters (size, plasma frequency, critical current), the condition of homogeneous irradiation over the array must be fulfilled. This requires a specific implementation of the junctions in an integrated circuit. Fig. 12 shows a 10 V array developed by PTB [64]. The array is made of 13 924 Nb/AlO_x/Nb junctions placed along a microstrip line which is divided in four arms of 3481 junctions in order to reduce the attenuation of the microwave radiation. A fine line antenna allows to couple the microwave (80 GHz) to the transmission line. For such an array, each junction typically operates on the 4th or 5th step over the 8 steps it can deliver and then the array provides a total voltage of 10 V, with steps equally spaced ($\Delta V = 165$ μV at 80 GHz), as shown on Fig. 13.

4.3.1. Josephson set-up

The typical experimental set-up developed by NMIs to calibrate their secondary standards (1.018 V Weston cells, 1 V and 10 V Zener diode references) against JAVS is sketched on Fig. 14. It consists in four parts and can be fully computer controlled:

- *The cryogenic part:* the array is mounted in a cryoprobe fitted with a low loss wave-guide. Three pairs of wires are used for visualizing the voltage steps, biasing the array with dc current and measuring the metrological voltage. The latter is filtered at the top against electromagnetic interference;
- *The microwave radiation source:* the circuit is constituted of a Gunn diode servo-controlled on a 10 MHz clock signal (rubidium crystal) by means of a phase-locked frequency counter and then referred to an atomic clock;
- *The electronics unit:* a dc current source is used to bias the array on the desired voltage step through an adjustable resistor placed in parallel;
- *The metrological circuit:* a digital nanovoltmeter coupled to a switch of low electromotive force measures the voltage difference between the JAVS and the device to be calibrated.

The typical uncertainties for a routine calibration of a Weston cell can be reduced down to a few tens of nanovolts [65]. In the case of a Zener diode reference, the calibration uncertainties are much degraded mainly due to their $1/f$ noise [66].

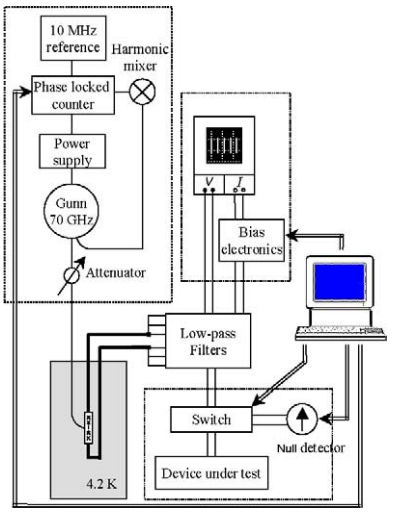

Fig. 14. Schematic of calibration set-up based on JAVS [67].

4.3.2. Comparisons

In the framework of the natural exercise of NMIs to check the coherence of their own standards, a large number of international comparisons involving 1 V and 10 V Josephson underdamped junction arrays has been performed [68]. The direct comparisons of JAVS are the most precise. In general, they show an agreement with an uncertainty of about one part in 10^{10}. Some comparisons with even smaller uncertainties have been reported [67,69]. A very good agreement, a few parts in 10^{10}, has also been found [70–72] in the recent comparisons involving the new generation of JAVS designed to be programmable as described below.

4.4. Programmable JAVS

Although 1 V and 10 V underdamped Josephson junction arrays provide NMIs with highly reproducible primary voltage standards, their working mode remains tricky and prevents other metrological applications. The voltage steps are not stable

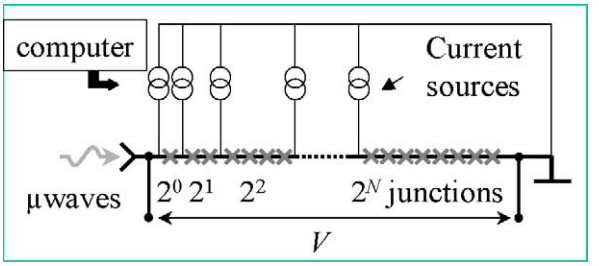

Fig. 15. Principle of binary-divided array. The highest segments are composed of 8192 (2^{13}) junctions so far.

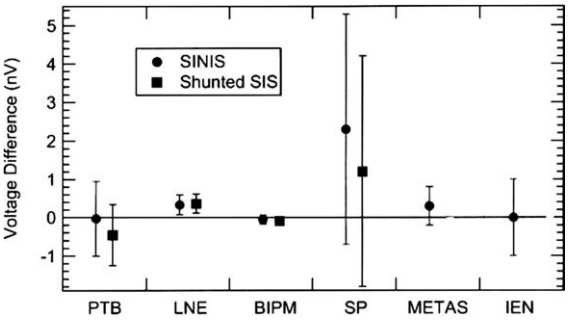

Fig. 16. Direct comparisons between binary arrays (SINIS or shunted SIS) with: another SINIS array (PTB), an SIS array (BNM-LNE, BIPM, IEN), an SNS array (METAS). Indirect comparison with an SIS array via Weston cells (SP) [72].

enough against environmental electromagnetic noise and they cannot be quickly and unambiguously settled. Consequently, a fully computer controlled calibration of Weston cells (without any risk of current flow) or a calibration of digital voltmeters is a difficult task. Generating arbitrary waveform ac voltage at audio frequency from these arrays is also not possible. These applications and others such as fast-reversed dc voltage measurements (for ac/dc testing of thermal converter [73], metrological triangle and Watt balance experiments), development of quantum voltmeter [74] and Josephson potentiometer [75], become possible by means of programmable arrays. These arrays, operating like a digital/analogue (D/A) converter, are of two types: binary-divided or pulse driven.

4.4.1. Binary-divided array

Invented by Hamilton et al. in 1995 [76], the array is divided into segments of M $(= 2^N)$ overdamped Josephson junctions, and each segment can be independently set to the $n = 0, \pm 1$ steps by applying on it the corresponding bias current $I_B = 0, \pm I$, and the microwave irradiation f (Fig. 15).

The output voltage of the array is the sum of the voltages developed at each segment, $V_{seg} = 0, \pm Mf/K_J$, and hence this allows the generation of any voltage from $-M_{tot}f/K_J$ to $+M_{tot}f/K_J$ per increment of $M_{min}f/K_J$, where M_{tot} is the total number of the junctions and M_{min} the number of junctions of the smallest segment.

In practice, the overdamped junctions are preferably made from SNS [77] or SINIS [78] (S superconductor, N normal, I insulator) technology, but externally shunted SIS junctions [79] can be used as well.

From these binary arrays, any arbitrary voltage might be adjusted without ambiguity and in a very short time, e.g. less than 1 μs. Moreover, the high critical current (1 mA for SNS or SINIS junctions compared with 100 μA at the most for SIS junctions) makes the voltage steps highly stable. However, because they occur at non-zero bias current, the voltage steps may be found sloped due to eventual small series resistance within the array [72]. The flatness has thus to be checked carefully [70,71].

Numerous direct comparisons between the different kinds of binary arrays and the conventional SIS arrays have been reported in literature. They have shown agreement better than 0.5 nV, or even within 0.1 nV, at 1 V level (Fig. 16) [70–72] or at voltage levels down to few tens of mV (by selecting small segments) [80]. Besides, a direct comparison of the voltages delivered by two segments, each composed of 4086 junctions, of a same SINIS array, has shown no difference at a level of 2 parts in 10^{17} [81].

All these results indicate that the programmable JAVS based on binary arrays will very likely replace conventional JAVS based on SIS arrays in near future.

In theory, the binary-divided array can also deliver ac voltages by selecting quickly and adequately voltage steps for each segment. The resulting signal is an approximate sinusoidal wave sampled by steps. However, during the period between two successive steps, the voltage is not quantized at all. This transience problem leads to errors on the rms value of the signal, which could be very important for metrological purposes [12]. Investigations are being pursued by NMIs to clarify this point [82].

4.4.2. Pulse driven array

In fact, an actual ac quantum voltage standard can be realised from a series array of overdamped Josephson junctions which, instead of being irradiated by sinusoidal microwaves, are driven with a train of short current pulses [83]. For a fixed repetition frequency of the pulse f, the time integrated value of the output voltage is $V = nNf/K_J$ where n is the step number which depends on the pulse height, and N the number of junctions.

In contrast to the case of sinusoidal excitation for which a frequency modulation induces a chaotic behaviour of the junction, or strongly affects the step width, the voltage steps do not depend on the frequency f if the pulse width $\tau_p = 1/(2\pi I_C R K_J)$ remains short enough: $\tau_p < 1/f$. Consequently, the output voltage of the array is easily adjustable by varying f.

Several NMIs [84,85] are developing Josephson arbitrary waveform synthesizer (JAWS) based on the principle of pulse drive. A digital code generator delivering pulses clocked at a high frequency (10 Gbit/s) in a predetermined sequence followed by a delta–sigma modulator used for D/A conversion allow to synthesize arbitrary waveforms (in the frequency range from dc up to 100 MHz). The rms voltage is calculable with a fundamental accuracy from the knowledge of the number of pulses and their positions in time. Promising results on synthesizing ac voltages with rms values higher than 100 mV have been reported by NIST [84]. They have shown that the errors (from 1 part to 30 parts in 10^4 in the frequency range from 1 to 50 kHz) arise mainly from the circuit (in particular from the used drive current) and few from the junctions. Improvement of circuits is thus needed in order to reduce the uncertainties under the expected level, i.e. less than 1 part in 10^6 at 1 kHz.

A promising alternative to the pulse driven array for generating ac voltages with a quantum precision is based on single flux quantum (SFQ) D/A converter [86–88]. The basic element of these devices is a superconducting loop closed by an overdamped Josephson junction (with $\beta_C = 1$). Each time the bias current exceeds the critical current of the junction, a single flux quantum Φ_0 crosses the loop and induces a short ($\approx$1 ps) voltage pulse for which the time integral is equal to Φ_0 exactly. Despite the simplicity of this SFQ logic, the realisation and fabrication of the SFQ D/A converters for a proper metrological use are rather complicated but remain possible. Recently, Semenov and Polyakov [89] reported encouraging results, i.e. first voltage measurements at a 100 mV level by means of such devices.

4.5. Determination of the Josephson and Planck constants

The Josephson constant K_J can be directly determined from an SI realisation of the volt. The principle consists in measuring the attraction force F between two electrodes, one fixed, and the other movable, on which a voltage drop U is applied. The measurement of U in terms of JE leads to an SI value of K_J:

$$K_J = nf\left(2F/(\mathrm{d}C/\mathrm{d}x)\right)^{-1/2}, \tag{13}$$

where n and f refer to the step number and the microwave frequency and $\mathrm{d}C/\mathrm{d}x$ is the variation of the capacitance between electrodes with their distance. $\mathrm{d}C/\mathrm{d}x$ is measured in SI with a Thompson–Lampard calculable capacitor. Two sets of apparatus have given rise to K_J values in 1980s, the liquid-mercury electrometer developed by CSIRO/NML and the voltage balance at PTB, with uncertainties around 3 parts in 10^7 [15]. Better uncertainties have been obtained by means of moving coil Watt balance. The experiment, described in more details in [16], consists in two successive phases:

- weighing (with a mass m) the Laplace force applied on a current (I) carrying coil in a magnetic flux,
- then measuring the electromotive force (U) created at the input of the same coil when it is moved in the same magnetic flux at constant speed (v). From these two phases the following relation results:

$$UI = mgv \tag{14}$$

which makes electrical and mechanical powers equivalent. The measurement of electrical quantities in terms of JE and QHE and that of mechanical quantities in SI units lead to an SI determination of the product $K_J^2 R_K$. If R_K is measured in SI elsewhere, then K_J is given in the simplified form:

$$K_J = f/(mgvR_K)^{1/2}. \tag{15}$$

The ultimate uncertainty expected on K_J by this method is of the order of one part in 10^8.

The Watt balance experiment combined with the SI realisation of the ohm consequently leads to the SI determination of the volt as well as of the ampere. Moreover, if the relations $K_J = 2e/h$ and $R_K = h/e^2$ are assumed exact, then the experiment gives access to a determination of the Planck constant:

$$h = 4/(K_J^2 R_K) = 4(mgv)/f^2. \tag{16}$$

Fig. 17 shows values of h determined until now by the Watt balances of NPL and NIST and values obtained by other electric means and by less direct methods (involving Faraday constant, shielded gyromagnetic ratio of proton in high field and molar volume of silicon) [15]. This indicates that the Watt balance is the technique of highest accuracy so far. It is noteworthy that these various measurements lead to the 2002 CODATA value $h = 6.62606693 \times 10^{-34}$ J s with a standard deviation uncertainty of 1.7 part in 10^7 and $K_J = K_{J\text{-}90}(1 - (4.3 \pm 8.5) \times 10^{-8})$ [15].

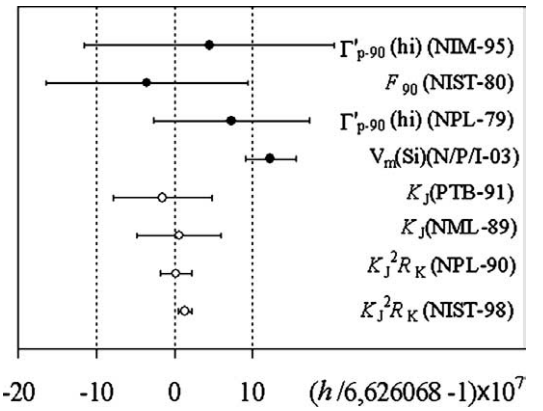

Fig. 17. Values of Planck constant determined by direct measurements (electrometer ad Watt balance) and by indirect methods [15].

Efforts have to be pursued for reducing the uncertainties on K_J (presently three orders of magnitude larger than the reproducibility of present-day JAVS) and h to a level of one part in 10^8. Moreover, once this onset value is reached, monitoring the kilogram for example by means of Watt balance will become a relevant task and would allow, in time, to redefine the kilogram by fixing the Planck constant. With this aim, NPL and NIST are improving their moving coil apparatus and, in the last few years, METAS [90] and then BNM [91] have been working on the development of new Watt balances.

5. Towards SET based standards

Although the ampere is the base electrical unit, its representation requires the volt and the ohm. This fact can be explained for a practical reason: the quantum-mechanical standards QHRS and JAVS enable one to achieve uncertainties much lower than experiment or artefact for a representation of the ampere realized up to now. However, a quantum current standard is developed in the framework of the metrological triangle experiment. The simplest idea imagined by physicists is a current source controlled electron by electron. For 15 years, the development of the nanofabrication has made it possible to create sub-micron devices that allow the manipulation of individual electrons. The SET devices consist of tunnel junctions in series forming isolated conductor pieces like 'metallic islands' on which the charge state is controlled by means of gate electrodes. The Coulomb blockade is the physical phenomenon, which originates from the SET devices and is described in the next section. In theory, a SET device like an electron pump can transfer millions of single charge through the circuit with an expected intrinsic uncertainty reaching one part in 10^9 and a SET electrometer can detect $\approx 10^{-5}e$ in a 1 Hz bandwidth. As a result, these systems have opened the path towards the realisation of quantum current standards based on highly accurate current sources (normal or Cooper pair pumps) or ultra-sensitive electrometers for making sensors or electrons counters (radio frequency (RF) SET transistor). A SET device constituted of pump servo-controlled by an electrometer enables one to realise a quantum capacitance standard as well.

After a few theoretical considerations about Coulomb blockade by taking the basic SET transistor as an example, various devices presently used in NMIs are described in the following subsections. The more promising devices are the electron pumps: connected to an external RF source generating a f frequency harmonic signal, a normal or superconducting pump transfers an integer number n (= 1 or 2 respectively) of electron charges per cycle. Consequently, the current amplitude is proportional to the elementary electron charge and the applied frequency: $I = nef$. A second way for developing a current standard is to combine a SET transistor with a RF resonant circuit. This so-called RF-SET device is a very sensitive single-electron electrometer and allows the very accurately counting of electrons crossing an array of junctions. Whereas the pump generates a current, the RF-SET device calibrates a current source. The SET-SAW device combining Coulomb repulsion and surface acoustic wave (SAW) effects is a quite different approach for making a standard source but remains a serious candidate.

5.1. The double junction and Coulomb blockade of tunnelling: SET transistor

The Coulomb blockade of electron tunnelling, observed for the first time in disorder granular materials [92], takes place in a SET device when a metallic *island* is electrically insulated from the rest of the circuit. If the total capacitance of the island C_Σ is sufficiently small compared to e^2/kT, the energy change required for the addition or subtraction of one electron on the island becomes high enough to prohibit the tunnelling transfer of the other electrons. The first remarkable feature of such a device is that the island consists of billions of electrons but remains sensitive to the presence of a single additional electron. Secondly,

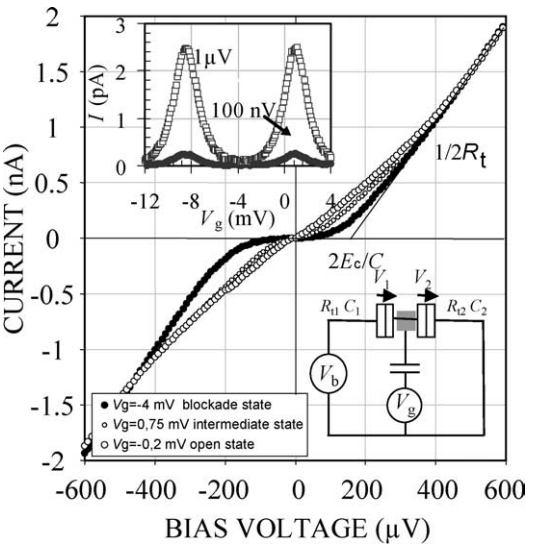

Fig. 18. I–V_b characteristics of SET transistor. Inserts: I–V_g characteristics and schematic view of the transistor.

the extra electron number on the island is necessarily an integer whereas $Q_{1,2}$, charges of the first or second junctions, can be fractional charges. When the thermally activated transport is suppressed (typically $T \ll 4$ K), the tunnelling of electrons through the circuit is possible under certain bias conditions.

The SET transistor (see insert Fig. 18) often used as an electrometer is the simplest SET device and consists of a single metallic island (usually aluminium) separated by thin insulating tunnel barriers (alumina) and coupled to a gate electrode through a capacitor (C_g). The energy needed for transferring an electron through the first or the second junction is the change of free energy $\Delta E^{\pm}_{1,2}$ of the complete circuit during the tunnelling:

$$\Delta E^{\pm}_{1,2} = \frac{e^2}{2C_\Sigma} \pm eV_{1,2} \tag{17}$$

with $V_{1,2} = Q_{1,2}/C_{1,2}$ where $C_{1,2}$ are capacitances of the first and second junction, respectively. From the equation above, the Coulomb energy, $E_c = e^2/(2C_\Sigma)$, is recognised. Moreover, tunnelling into an unoccupied state is possible if the electron gains kinetic energy coming from the decrease of the electrostatic energy of the system, and thus a threshold voltage occurs:

$$\Delta E^{\pm}_{1,2} \leqslant 0 \Rightarrow |V_b| \geqslant V_t = \frac{e}{C_\Sigma}. \tag{18}$$

As shown in Fig. 18 (insert), the transport properties of the transistor change periodically with the gate voltage V_g, or, in other words, with the charge state of the island. The period corresponds to an addition of one electron to the island. V_g can be adjusted such that the electron transfer through the device is blocked and so the current is zero. Consequently, the tunnelling can be stopped thanks to two parameters: V_g and V_b.

Fig. 18 also shows the measured I–V characteristic for a SET transistor with symmetrical junctions ($C_1 = C_2 = C_\Sigma/2$) and for three gate voltages where the Coulomb gap is maximum, minimum and intermediate. In the case of blockade state, the conduction below the threshold voltage ($V_t = e/C_\Sigma$) is close to zero. By changing the gate voltage, the Coulomb gap can be completely suppressed and the curve appears almost linear.

5.2. The R-pump

The SET pump, first investigated by Pothier et al. [93] is a device allowing the transfer of electrons one by one at an adjustable clock frequency f, and in a quasi-adiabatic way. The electric current through the electron pump can be expressed by: $I = e \cdot f$. The simplest electron pump consists of two metallic *islands* separated by three junctions (actually $C_1 = C_2 = C_3$). The gate voltages V_{G1} and V_{G2} through the gate capacitance C_{G1} and C_{G2} can control the electric potential of each island. The pump operation can be illustrated by means of the typical diagram given in Fig. 19, which displays the stability domains of the different states (n_1, n_2) in the $V_{g1} \otimes V_{g2}$ plane. The integer couple (n_1, n_2) denotes the number of extra charges present on the first and the second island. The points (Fig. 19), so-called triple points, where conduction can take place are located at the intersection of three neighboring domains. Everywhere else, the pump is in a blockade state and the electron configuration

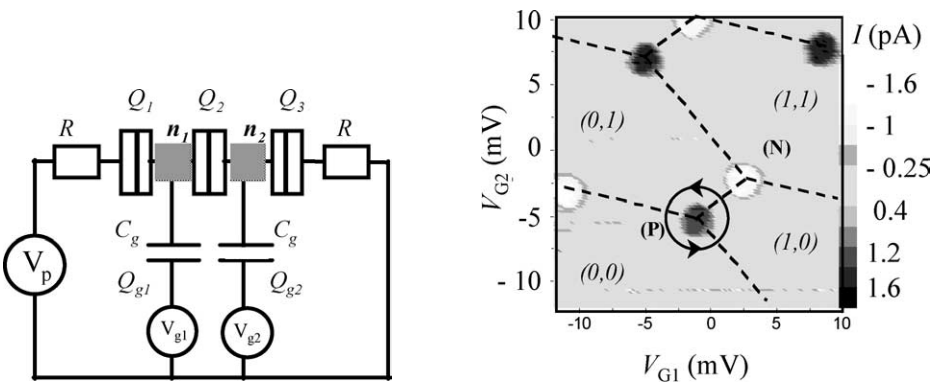

Fig. 19. Right: schematic view of a R-pump device. Left: stability diagram in $V_{g1} \otimes V_{g2}$ plane which displays the stable configurations (n_1, n_2) of numbers of the extra electrons on each island. Boundaries between each domains (dashed lines) form a typical honey-comb pattern. The charges tunneling transfer as a function of gate voltages V_{G1} and V_{G2} takes place only in the triple points regions [94]. This diagram has been obtained at BNM-LNE by means of a CCC used as a current amplifier [95,96].

(n_1, n_2) is stable. Dashed lines represent the boundaries between each stability domains and form a typical honey-comb pattern. The pumping of electrons is based on these topological properties.

The controlled transfer of electrons is obtained in the following way: two periodic signals with the same frequency f but phase shifted by $\Phi \approx 90°$ are superimposed on each applied dc gate voltage couple (V_{g10}, V_{g20}) as following:

$$V_{g1} = V_{g10} + A\cos(2\pi f t),$$
$$V_{g2} = V_{g20} + A\cos(2\pi f t + \Phi)$$

When the dc voltages (V_{g10}, V_{g20}) correspond to coordinates of the point denoted P, the circuit follows a closed trajectory around P as shown in Fig. 19. The configuration changes from $(0, 0)$ to $(1, 0)$, then from $(1, 0)$ to $(0, 1)$, and returns to the initial state $(0, 0)$. In the real space, the complete sequence involves the transfer of one electron throughout the R-pump.

The frequency is chosen low compared to the reciprocal of the tunnel rate ($f \ll R_j C$, R_j is the junction resistance). This condition ensures that the system adiabatically returns to its ground state. By adding 180° to the phase shift Φ, the rotation sense is reversed in configuration space, and the electron by electron current takes place in the opposite direction [94].

The cross-capacitance effect can be eliminated by means of an electronic device connected to both gate wiring inputs which adds a fraction of the voltage applied to one gate to the other gate, with opposite polarity [97].

The accuracy of the charge transfer is partly limited by the co-tunnelling effect. This phenomenon involves simultaneous tunnelling of electrons from islands through each junction. In order to avoid errors in the transport rate, increasing the number of the junctions is a first solution. However, PTB has proposed to keep 3-junction pumps, the easiest to use, and to place on-chip resistive Cr-microstrips of typically 50 kΩ in series with the pump [98], thus named an R-pump (Fig. 20). As a result, dissipation of electron tunnelling energy in the resistors suppresses undesirable effects of co-tunnelling and an increased accuracy can be achieved.

The I–V_b curve given in Fig. 21 and so-called current step illustrates the current stability with bias conditions. This characteristic is determining for the development of current standards. Thus, stable current on 300 μV in a 40 fA range was obtained with a PTBs R-pump connected to a CCC. An investigation on long time measurements has shown that these pumps were able to generate a current $I = ef$ during more than 12 hours [94].

5.3. The Cooper pair pump

In principle, the devices consisting of small-capacitance Josephson junctions forming superconducting islands coupled to gate electrodes are able to pump Cooper pairs one-by-one driven by a frequency higher than in the *normal* pump case. However, the tunnelling of Cooper pairs is a phenomenon more complex than that of electrons in the normal state because the Josephson coupling energy, E_J $(= \hbar I_C/2e)$, must be taken into account and compared directly to the charging energy, E_c. Nevertheless, with $E_J < E_c$, a current $I = \pm 2ef$ generated by a three-junctions superconducting pump has been observed by several authors [99–101]. But, the transfer of the Cooper pairs across the device is disturbed by factors (Cooper pair co-tunnelling, quasi-particles poisoning, ...) involving an imperfect plateau of the I–V curve. In order to improve the accuracy of the superconducting pumps, Zorin et al. have proposed to connect resistors in series to the ends of the array following the example of

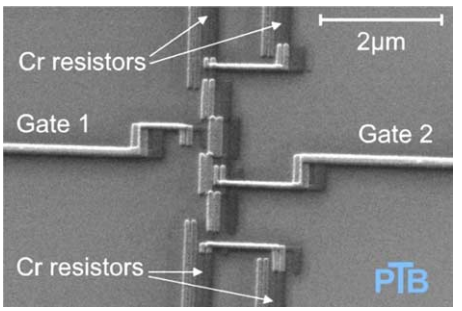

Fig. 20. SEM-image of 3-junctions R pump fabricated by PTB [98] (illustration by courtesy of the PTB).

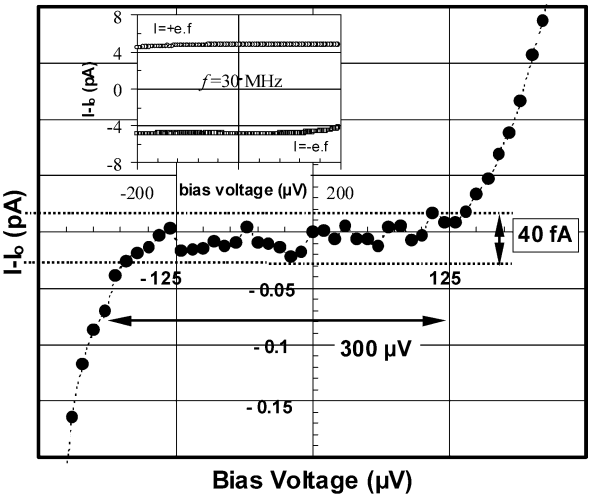

Fig. 21. Current step with an R-pump operating at 10 MHz (in insert: current steps at 30 MHz). These steps have been obtained with the BNM-LNE CCC for a short measurement time (5 min) [94].

their R-type normal pumps [101]. The measurements show the through-supercurrent and the unwanted co-tunnelling events are dramatically suppressed.

5.4. The RF-SET transistor

The bandwidth of a classical SET transistor used as an electrometer is typically around 1 kHz and can achieve 1 MHz with some improvements. However, it is too low to detect a 1 pA current with a metrological accuracy, which requires a bandwidth of 10 MHz at least. Therefore, following the principle of the SQUID technology, a SET transistor is connected with a resonant circuit. Such a device, called RF-SET, capacitively coupled to a long array of tunnel junctions, makes the electrons counting one-by-one possible [102]. In a long array of tunnel junctions, charges flow in the form of regularly spaced solitons. Electrons generated by an external current source penetrate into the array of junctions and change the charging state of the island of the transistor when they come close to it. An incident RF signal is partially absorbed by the RF-SET if the transistor is in the open state or totally reflected in the blockade state. Consequently, this system is able to detect the crossing of an individual electron by counting each change of state. In principle, the aim should be to reach a counting speed of at least 60 MHz, corresponding to 10 pA with a 10 parts in 10^6 uncertainty.

5.5. SET-SAW

The principle and the design of the electron transfer using a surface acoustic wave (SAW) generating a quantized current is quite different from the one of the pumps, but the SET-SAWs remain interesting candidates for developing a current standard source or for quantum computing. A 2DEG in a heterostructure of GaAs/AlGaAs, very similar to those present within QHE devices, is confined to a one-dimensional channel by using split-gate technique. Thus, this channel is located between two electron reservoirs. By applying an appropriate voltage to the gate, the electron density in the constriction can be reduced to zero and an energy barrier for electrons appears. Due to the piezoelectric effect, a potential modulation is created, propagates through the SET-SAW and is superimposed on the energy barrier in the constriction area. Based on the Coulomb repulsion, it has been shown that an integer number of electrons, determined by the created well size, can be transferred through a SET-SAW device and generates a current $I = Nef$ [103]. The maximum speed would be around 10 GHz. But, the accuracy of SET-SAW devices is limited by the overheating of electrons due to RF power needed by the transducer and by the speed of switching on and off of the propagating acoustic wave [104]. For several years, collaboration between University of Cambridge and NPL has extensively investigated and developed a SET-SAW current standard [105]. A total current uncertainty of a few parts in 10^4 has been estimated but no real flat plateau has been displayed [106].

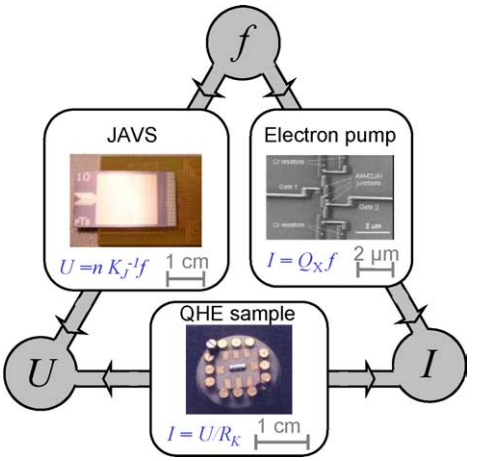

Fig. 22. Quantum metrological triangle (photographs of programmable JAVS and electron pump by courtesy of the PTB).

6. Quantum metrological triangle

The single charge tunnelling could provide the missing link of the quantum metrological triangle (QMT) [19] (Fig. 22) by realising a quantum current standard and, as described below, an electron counting capacitance standard (ECCS).

The closure of the QMT experimentally consists in applying $U = RI$ or $Q = CV$, directly from SET, JE and QHE. In practice, the experiment comes down to determine the dimensionless product $R_K K_J Q_X$, expected to be equal to 2, where the constant Q_X is defined as an estimate of the elementary charge [20], $Q_X = e|_{SET}$, by analogy to the definitions of Josephson and von Klitzing constants. Checking the equality $R_K K_J Q_X = 2$ with an uncertainty of one part in 10^8 will be a relevant test of the validity of the three theories.

The high level of agreement shown by numerous comparisons of quantum resistance and voltage standards involving so different kinds of devices undoubtedly strengthens our confidence in the universal and fundamental aspects of K_J and R_K and hence in the equalities $K_J = 2e/h$ and $R_K = h/e^2$. However, even if strong theoretical arguments exist, from a strictly metrological point of view, these relations are not proven. The exactness of these two relations has been recently tested by the CODATA Task group in the framework of the 2002 fundamental constant adjustment. It is shown that there is no significant deviation between K_J and $2e/h$ and between R_K and h/e^2, but within a fairly large uncertainty in the case of Josephson relation. The uncertainties amount to 8 and 2 parts in 10^8 respectively [15].

6.1. $U = RI$ and current amplification

The QMT experiment proposed by BNM-LNE [20], consists in the direct comparison of the voltage U_J supplied by a Josephson junctions array to the Hall voltage of a QHE sample crossed by a current I delivered by a SET current source and amplified by means of a CCC [95,96]. This comparison leads to the relation:

$$U_J = R_H N_{CCC} I, \tag{19}$$

where N_{CCC} is the CCC winding ratio. Considering the JE, QHE and SET relationships, Eq. (19) becomes:

$$n f_J / K_J = (R_K / i) N_{CCC} Q_X f_{SET}, \tag{20}$$

where n is the index of the voltage step delivered by the JAVS at the microwave frequency f_J, i is the index of the QHE plateau and f_{SET} is the driving frequency of the SET current source. It leads to the dimensionless product:

$$R_K K_J Q_X = n(i/N_{CCC}) f_J / f_{SET}. \tag{21}$$

Measuring the deviation of $R_K K_J Q_X$ from 2 will give information on the consistency level of the three quantum phenomena. It is noteworthy that the ratio Q_X/e will be determined if one assume $R_K = h/e^2$ and $K_J = 2e/h$ and Q_X may be estimated in terms of $R_{K\text{-}90}$ and $K_{J\text{-}90}$ with an expected value of $2/(R_{K\text{-}90} K_{J\text{-}90}) = 1.60217649 \times 10^{-19}$ C.

The required CCC for amplifying the very small current generated by an electron pump must present a high winding ratio and ultra low noise performances. In this framework some CCCs have been investigated by NMIs. The one made by BNM-LNE and firstly used for measuring SET device [92] has a winding ratio N_1/N_2 of 10 000. Its noise spectral density is 4 fA/Hz$^{1/2}$

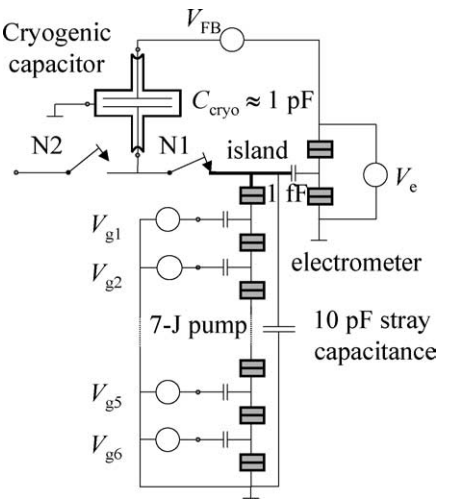

Fig. 23. Principle of electron counting capacitance standard [108].

in the white noise range ($f > 0.5$ Hz). It allows measurements of currents from 1 pA to a few nA, with a type A uncertainty of 50 aA for a one hour measurement [95]. With this system, the current of 3.2 pA supplied by an electron pump has been measured with an uncertainty of 600 aA (i.e. a relative uncertainty of 1.9 parts in 10^4) after 15 hours of measurement [107]. From this result, some improvements have to be made in order to attempt an ultimate uncertainty of 1 part in 10^8. SET devices capable to supply currents up to 100 pA and generating lower noise must be developed. A new amplifier with a better sensitivity is also needed. This can be obtained by increasing the CCC gain with a factor 5 and by using a SQUID well suited to the experiment.

6.2. $Q = CU$ and electron counting capacitance standard

The development of a capacitance standard from SET devices is feasible by applying the natural definition of the capacitance: the transfer of a well-known charge Q between the electrodes of a capacitor with a capacitance C and the measurement of the potential difference ΔV between these electrodes: $C = Q/\Delta V$.

Fig. 23 exhibits a schematic view of the operational experimental system developed by NIST [108]. Similar systems are developed by other NMIs (METAS, NMi/VSL, NPL, PTB).

The NIST system consists of a seven junction electron pump, a SET transistor/electrometer with a charge detection threshold of the order of $e/100$, and a cryogenic capacitor built with a specific attention on leakage currents and frequency and temperature effects. Two mechanical cryogenic switches N_1 and N_2 allow two working phases (Fig. 23).

6.2.1. N_1 *closed,* N_2 *open*

In this phase, the cryogenic capacitance C_{cryo} ($\approx$1 pF) is charged with N electrons generated one by one through the pump. The process is stopped for a short time (20 s) to measure the voltage V_c^+. Then, the pump is forced to transfer N electrons in the opposite direction. Another stop occurs to measure a voltage V_c^-, and so on. The successive voltages V_c^+ and V_c^- are compared to those of a JAVS and the differences $\Delta V = V_c^+ - V_c^-$ are calculated. The average of these differences $\langle \Delta V \rangle$ gives the capacitance:

$$C_{cryo} = Ne/\langle \Delta V \rangle = (N/nf_J)K_J Q_X \tag{22}$$

from the relation $\langle \Delta V \rangle = nf_J/K_J$ where n is the index of the voltage step provided by the binary Josephson array at a frequency f_J. Up to now, the best relative standard deviation of C_{cryo} values obtained with electron counting is of the order of a few parts in 10^7 [108].

6.2.2. N_1 *open,* N_2 *closed*

In this second configuration, C_{cryo} is compared with the capacitance C_X of a capacitor at room temperature using a capacitance bridge. Three kinds of results could be obtained:

1. If C_X has been previously calibrated in relation to the second and R_K with a quadrature bridge, it can be written in a simplified form as:

$$C_X = 1/(2\pi R_K f_q), \tag{23}$$

where f_q is the balance frequency of the bridge. Combining relationships (22) and (23) and giving up the integer numbers leads to a new expression of the dimensionless product $R_K K_J Q_X$:

$$R_K K_J Q_X = (C_{cryo}/C_X) f_J/f_q. \tag{24}$$

The capacitance ratio in this relationship is measured at a frequency in the kHz range (f_q), much higher than the effective frequency of electron counting (25 mHz). Consequently, the frequency dependence of the cryogenic capacitor must be very small or well known. Voltage and drift effects might also affect the experiment. Unlike the $U = RI$ approach, this experiment does not need a SET source supplying currents higher than a few pA.

2. If the capacitance C_X is directly compared to the calculable capacitor, so in terms of SI units, $C_X = C_{X,SI}$, and a SI value of the product $K_J Q_X$ can be deduced:

$$K_J Q_X = (C_{cryo}/C_X) f_J C_{X,SI}. \tag{25}$$

The combination with the closure of the triangle via $U = RI$ leads to a new SI realisation of R_K. The relations (21) and (25) give:

$$R_K = (C_X/C_{cryo})(f_J/f'_J)(f_{SET} C_{X,SI})^{-1}. \tag{26}$$

The relations (25) and (26) give rise to two new determinations of α with the assumptions $R_K = h/e^2$, $K_J = 2e/h$ and $Q_X = e$. It is noteworthy that the first one is independent of QHE.

3. If the capacitance C_X is unknown, then the comparison with C_{cryo} acting as a standard becomes a calibration. From (24) assuming the equality $R_K K_J Q_X = 2$ to be right and considering the recommended value $R_{K\text{-}90}$, a simplified expression of C_X can be deduced:

$$C_X = 1/(2\pi R_{K\text{-}90} f_J). \tag{27}$$

This relation is similar to (23) except for the frequency. Using a conventional commercial bridge to measure the capacitance ratio, Keller et al. have shown that the relative deviation between the value of C_X deduced from this method and the one deduced from a classical calibration is only 5 parts in 10^7. This deviation is insignificant, considering the calibration uncertainty of the bridge (1 part in 10^6) [108]. In the future, this quantum calibration of a capacitance could be made with a relative uncertainty of 1 part in 10^7. However, the calibration of a capacitance in terms of QHR, given by (22), is a serious alternative considering that uncertainties of one part in 10^7 or less have already been reached.

As a conclusion, it is shown that the QMT experiments do not consist solely in verifying the consistency of QHE, JE and SET. The closure of QMT via the two approaches $U = RI$ or $Q = CU$, with an uncertainty of one part in 10^8 will give significant information that can be taken into account when adjustment are made to the fundamental constants. Combined with measurements of cryogenic capacitance in SI units, the QMT experiments lead to new observational equations given by (21), (24), (25) and (26). Using the same notations as in [15], these equations are rewritten as follows:

$$Q_{X\text{-}90} \doteq \left[(K_J R_K)/(K_{J\text{-}90} R_{K\text{-}90})\right]\left[2\alpha h/(\mu_0 c)\right]^{1/2},$$
$$K_J Q_X \doteq 4\alpha/\mu_0 c,$$
$$R_K \doteq \mu_0 c/2\alpha,$$

where $Q_{X\text{-}90} = [I \times A/A_{90}]/f$. The equality symbol indicates the measured quantity (left term) is ideally given by the function of the adjusted constants (right term).

7. Conclusions and prospects

Replacing the International System of units (SI) by a new SI based on fundamental constants is the general trend of the metrological community. Through the universal constants, this new SI creates a direct link between fundamental physics and units.

Since more than one decade, quantum-mechanical standards such as JAVS and QHRS have fully solved the problem of multiple representations based on previous artefact standards (standard cells and 1 Ω resistor). They present advantages in being highly stable in time and based on well-established physical laws implying fundamental constants in a simple way.

On the other hand, the implementation in metrology of these experiments allowing the determination of the constants involved and the check of their consistency with quantum metrological triangle experiments, contributes to an important improvement in the physics phenomena knowledge by verifying theories and fundamental assumptions. All the prospects in this domain are conceivable and some of them might be a real disruption of our points of view on nature: what would happen if experiments prove any amazing result, challenging some of our beliefs? That is what makes quantum metrological experiments an extremely exciting work.

Although the industrial economic community has already taken advantage of the new developments which have occurred in NMIs due to QHE and JE, this will go on in an increasing way. For this aim, some axes of research have to be pursued in both quantum phenomena. Indeed, the availability of QHARS on the one hand and JAVS on the other hand, will make possible the use of such devices even by calibration centres in their routine work. QHARS is one of these axes because of the extended range of resistances and the higher measuring currents that can be allowed, making them compatible with commercial bridges. Other fundamental developments are possible as quantum impedance standard from ac QHR or JAVS for improving ac measurements of low voltage in the audio frequency range, instead of the thermal transfer method.

The development of the Coulomb blockade nanodevices opens extended prospects for applications in fundamental electrical metrology (current and capacitance standards, QMT experiments). These nanodevices also present a high metrological potential in the applied domain of electricity and ionising radiation (calibration of sub-nano ammeters and development of charge detector), in thermometry (absolute cryogenic thermometer with so-called Coulomb blockade thermometer), in nanometrology (nanometer scale displacement sensor) and in new fields based on single photon sources (single or multiple photon discrimination metrology, quantum cryptography and computing). Moreover, in contrast to QHE and JE, some encouraging preliminary results and the advances in nanofabrication techniques (miniaturization of the tunnel junction) will make feasible SET devices operating at room temperature in the future.

Acknowledgement

We gratefully thank S. Djordjevic and W. Poirier for their helpful advice.

References

[1] J. Kovalevsky, T.J. Quinn, C. R. Physique 5 (2004), in this issue.
[2] A.M. Thompson, D.G. Lampard, Nature 177 (1956) 888–890.
[3] K. von Klitzing, G. Dorda, M. Pepper, Phys. Rev. Lett. 45 (6) (1980) 494–497.
[4] R.E. Prange, S.M. Girvin (Eds.), The Quantum Hall Effect, second ed., Springer-Verlag, New York, 1990.
[5] M. Stone, Quantum Hall Effect, World Scientific, Singapore, 1992.
[6] A. Hartland, Metrologia 29 (2) (1992) 175–190.
[7] F. Piquemal, Bull. BNM 116 (1999) 5–57.
[8] B. Jeckelmann, B. Jeanneret, Rep. Prog. Phys. 64 (2000) 1603–1655.
[9] B.D. Josephson, Phys. Lett. 1 (1962) 251–253;
B.D. Josephson, Rev. Mod. Phys. 36 (1964) 216–220.
[10] J.C. Gallop, SQUIDs, the Josephson Effects and Superconducting Electronics, Adam Hilger, Bristol, 1990.
[11] R. Pöpel, Metrologia 29 (2) (1992) 153–174.
[12] C.A. Hamilton, C.J. Burroughs, S.P. Benz, IEEE Trans. Appl. Supercond. 17 (2) (1997) 3756–3761.
[13] J. Kohlmann, R. Behr, T. Funck, Meas. Sci. Technol. 14 (2003) 1216–1228.
[14] B.W. Petley, Metrologia 29 (2) (1992) 95–112.
[15] P.J. Mohr, B.N. Taylor, CODATA recommended values of the fundamental physical constants: 2002, Rev. Mod. Phys. 76 (4) (2004) in press;
2002 CODATA values available on: http://www.physics.nist.gov/constants.
[16] W. Schwitz, B. Jeckelmann, P. Richard, C. R. Physique 5 (2004), in this issue.
[17] H. Grabert, M.H. Devoret (Eds.), Single charge tunneling Coulomb blockade phenomena in nanostructures, NATO Adv. Sci. Inst. Ser. B Phys., vol. 294, Plenum Press, New York, 1991.
[18] M.W. Keller, in: Recent Advances in Metrology and Fundamental Constants, Proceedings of Fermi School CXLVI, Vérone, 2000.
[19] K. Likharev, A. Zorin, J. Low Temp. Phys. 59 (1985) 347–382.
[20] F. Piquemal, G. Genevès, Metrologia 37 (2000) 207–211.
[21] C. Bordé, BIPM Summer School, Sèvres, private communication, 2003.
[22] W.K. Clothier, Metrologia 1 (2) (1965) 35–56.
[23] G. Trapon, O. Thévenot, J.C. Lacueille, W. Poirier, H. Fhima, G. Genevès, IEEE T. Instrum. Meas. 50 (2) (2001) 572–575.
[24] G. Trapon, O. Thévenot, J.C. Lacueille, W. Poirier, Metrologia 40 (2003) 159–171.
[25] CIPM, Rapport de la 22ème session du CCEM, 89ème session, octobre 2000, p. 34.

[26] CIPM, Représentation de l'ohm au moyen de l'effet Hall quantique, Recommandation 2 (CI-1988), 77ème session, octobre 1988.
[27] F. Piquemal, G. Genevès, F. Delahaye, J.P. André, J.N. Patillon, P. Frijlink, IEEE T. Instrum. Meas. 42 (2) (1993) 264–268.
[28] R.B. Laughlin, Phys. Rev. B 23 (10) (1981) 5632–5633.
[29] M. Büttiker, Phys. Rev. B 38 (1988) 9375–9389.
[30] F. Delahaye, B. Jeckelmann, Metrologia 40 (2003) 217–223.
[31] A. Hartland, K. Jones, J.M. Williams, B.L. Gallagher, T. Galloway, Phys. Rev. Lett. 66 (1991) 969–973.
[32] B. Jeckelmann, A.D. Inglis, B. Jeanneret, IEEE T. Instrum. Meas. 44 (1995) 269–272.
[33] F. Delahaye, T.J. Witt, F. Piquemal, G. Genevès, IEEE T. Instrum. Meas. 44 (1995) 258–261.
[34] Data available on BIPM website: http://www.bipm.fr/.
[35] A. Satrapinski, H. Seppä, B. Schumacher, P. Warnecke, F. Delahaye, W. Poirier, F. Piquemal, IEEE T. Instrum. Meas. 50 (2001) 238–241.
[36] M. Nakanishi, J. Kinoshita, T. Endo, Z. Zhang, H. Shao, Q. He, B. Liang, Metrologia 39 (2002) 207–212.
[37] W. Poirier, F. Piquemal, H. Fhima, N. Bensaïd, G. Genevès, in: Proc. of 9ème Congrès International de Métrologie, Bordeaux, 1999.
[38] A.D. Inglis, in: Conf. Digest CPEM 2004, London, 2004, in press.
[39] J.C. Gallop, F. Piquemal, SQUIDS for standards and metrology, in: J. Clarke, A. Braginski (Eds.), SQUIDS Handbook, chapter 9, Wiley, Berlin, in press.
[40] I.K. Harvey, Rev. Sci. Instrum. 43 (1972) 1626–1629.
[41] D.B. Sullivan, R.F. Dziuba, Rev. Sci. Instrum. 45 (1974) 517–519.
[42] F. Delahaye, IEEE T. Instrum. Meas. 27 (1978) 426–429.
[43] F. Delahaye, J. Appl. Phys. 73 (1993) 7914–7920.
[44] F. Piquemal, J. Blanchet, G. Genevès, J.P. André, IEEE T. Instrum. Meas. 48 (2) (1999) 296–300.
[45] W. Poirier, A. Bounouh, K. Hayashi, H. Fhima, F. Piquemal, G. Genevès, J.P. André, J. Appl. Phys. 92 (2002) 2844–2854.
[46] W. Poirier, A. Bounouh, F. Piquemal, J.P. André, in: Conf. Digest CPEM 2002, Ottawa, 2002, pp. 534–535.
[47] W. Poirier, A. Bounouh, F. Piquemal, J.P. André, Metrologia 41 (2004) 285–294.
[48] A. Bounouh, W. Poirier, F. Piquemal, G. Genevès, J.P. André, IEEE T. Instrum. Meas. 52 (2) (2003) 555–558.
[49] F. Delahaye, B.P. Kibble, A. Zarka, Metrologia 37 (2000) 659–670.
[50] Delahaye F., Rapport BIPM-2001/01.
[51] F. Overney, B. Jeanneret, B. Jeckelmann, IEEE T. Instrum. Meas. 52 (2) (2003) 574–578.
[52] J. Melcher, et al., IEEE T. Instrum. Meas. 52 (2) (2003) 563–568.
[53] S. Shapiro, Phys. Rev. Lett. 11 (1963) 80–82.
[54] F. Bloch, Phys. Rev. B 2 (1970) 109–121.
[55] J.S. Tsai, A.K. Jain, J.E. Lukens, Phys. Rev. Lett. 51 (4) (1983) 316–319.
[56] CIPM, Représentation du volt au moyen de l'effet Josephson, Recommandation 1 (CI-1988), 77ème session, octobre 1988.
[57] W.C. Stewart, Appl. Phys. Lett. 12 (8) (1968) 277–280.
[58] D.E. Mc Cumber, J. Appl. Phys. 39 (7) (1968) 3113–3118.
[59] H. Rogalla, Josephson junctions, in: B. Seeber (Ed.), Handbook of Applied Superconductivity, Bristol, 1998, pp. 1759–1775.
[60] A.M. Kadin, Introduction to Superconducting Circuits, Wiley, New York, 1999.
[61] M.T. Levinson, R.Y. Chiao, M.J. Feldman, B.A. Tucker, Appl. Phys. Lett. 31 (1977) 776–778.
[62] J. Niemeyer, J.H. Hinken, R.L. Kautz, Appl. Phys. Lett. 45 (1984) 478–480.
[63] C.A. Hamilton, F.L. Lloyd, K. Chieh, W.C. Goeke, IEEE T. Instrum. Meas. 38 (2) (1989) 314–316.
[64] R. Pöpel, J. Niemeyer, R. Fromknecht, L. Meier, L. Grimm, F.W. Dünschede, IEEE T. Instrum. Meas. 40 (2) (1991) 298–300.
[65] C.A. Hamilton, Y.H. Tang, Metrologia 36 (1999) 53–58.
[66] T.J. Witt, IEEE T. Instrum. Meas. 52 (2) (2003) 487–490.
[67] J.P. Lo-Hive, G. Genevès, Bull. BNM 111 (1998) 3–12.
[68] D. Reymann, T.J. Witt, IEEE T. Instrum. Meas. 42 (2) (1993) 596–599.
[69] D. Reymann, T. Witt, G. Eklund, H. Pajander, H. Nilsson, R. Behr, T. Funck, F. Müller, IEEE T. Instrum. Meas. 48 (2) (1999) 257–261.
[70] B. Jeanneret, A. Rüfenacht, C.J. Burroughs, IEEE T. Instrum. Meas. 50 (2) (2001) 188–191.
[71] R. Behr, H. Schulze, F. Müller, J. Kohlmann, J. Niemeyer, IEEE T. Instrum. Meas. 48 (2) (1999) 270–273.
[72] R. Behr, et al., IEEE T. Instrum. Meas. 52 (2) (2003) 524–528.
[73] C.J. Burroughs, S.P. Benz, C.A. Hamilton, T.E. Harvey, J.R. Kinard, T.E. Lipe, H. Sasaki, IEEE T. Instrum. Meas. 48 (1999) 282–284.
[74] R. Behr, et al., IEEE T. Instrum. Meas. 50 (2001) 185–187.
[75] R. Behr, T. Funck, B. Schumacher, P. Warnecke, IEEE T. Instrum. Meas. 52 (2) (2003) 521–523.
[76] C.A. Hamilton, C.J. Burroughs, R.L. Kautz, IEEE T. Instrum. Meas. 44 (1995) 223–225.
[77] C.J. Burroughs, S.P. Benz, T.E. Harvey, C.A. Hamilton, IEEE T. Appl. Supercond. 9 (1999) 4145–4149.
[78] J. Kohlmann, H. Schulze, R. Behr, I.Y. Krasnopolin, F. Müller, J. Niemeyer, in: Applied Superconductivity, Inst. Phys. Conf. Ser. 167 (2000) 769–772.
[79] J. Hassel, H. Seppä, L. Gronberg, I. Suni, IEEE T. Instrum. Meas. 50 (2001) 195–198.
[80] J.P. Lo-Hive, et al., IEEE T. Instrum. Meas. 52 (2) (2003) 516–520.
[81] I.Y. Krasnopolin, R. Behr, J. Niemeyer, Supercond. Sci. Technol. 15 (7) (2002) 1034.
[82] J. Williams, et al., in: Conf. Digest CPEM 2002, Ottawa, 2002, pp. 434–435.
[83] S.P. Benz, C.A. Hamilton, Appl. Phys. Lett. 68 (1996) 3171–3173.
[84] C.J. Burroughs, S.P. Benz, P.D. Dresselhaus, IEEE T. Instrum. Meas. 52 (2) (2003) 542–544.
[85] O. Chevtchenko, et al., in: Conf. Digest CPEM 2004, London, 2004.

[86] C.A. Hamilton, IEEE T. Appl. Supercond. 2 (1992) 139–142.
[87] V.K. Semenov, IEEE T. Appl. Supercond. 3 (1993) 2637–2640.
[88] H. Sazaki, S. Kiryu, F. Hirayama, T. Kikuchi, M. Maezawa, A. Shoji, IEEE T. Appl. Supercond. 2 (1999) 3561–3564.
[89] V.K. Semenov, Yu.A. Polyakov, IEEE T. Appl. Supercond. 11 (2001) 550–553.
[90] W. Beer, et al., IEEE T. Instrum. Meas. 50 (2) (2001) 583–586.
[91] G. Genevès, et al., in: Conf. Digest CPEM 2004, London, 2004.
[92] H.R. Zeller, I. Giaver, Phys. Rev. 181 (1969) 789.
[93] H. Pothier, P. Lafarge, P.F. Orfila, C. Urbina, D. Esteve, M.H. Devoret, Physica B 169 (1991) 573–574.
[94] N. Feltin, L. Devoille, F. Piquemal, S. Lotkhov, A. Zorin, IEEE T. Instrum. Meas. 52 (2003) 599–603.
[95] F. Gay, PhD Thesis, Conservatoire des Arts et Métiers, Paris, France, 2000.
[96] F. Gay, F. Piquemal, G. Genevès, Rev. Sci. Instrum. 71 (2000) 4592–4595.
[97] M.W. Keller, J.M. Martinis, N.M. Zimmerman, A.H. Steinbach, Appl. Phys. Lett. 69 (1996) 1804–1806.
[98] S.V. Lotkhov, S.A. Bogoslovsky, A.B. Zorin, J. Niemeyer, Appl. Phys. Lett. 78 (2001) 946–948.
[99] D.V. Averin, K.K. Likharev, Single-electronics: correlated transfer of single electrons and Cooper pairs in small tunnel junctions, in: B.L. Alsthuler, P.A. Lee, R.A. Webb (Eds.), Mesoscopic Phenomena in Solids, North-Holland, Elsevier, Amsterdam, 1991, pp. 173–271.
[100] L.J. Geerligs, et al., Z. Phys. B 85 (1991) 349.
[101] A.B. Zorin, S.A. Bogoslovsky, S.V. Lotkhov, J. Niemeyer, cond-mat/0012177, 2000, v1.
[102] R.J. Schoelkopf, P. Wahlgren, A.A. Kozhevnikov, P. Delsing, D.E. Prober, Science 280 (1998) 1238–1242.
[103] J.M. Shilton, et al., J. Phys. Cond. Matt. 8 (1996) L531–L539.
[104] J. Ebbecke, N.E. Fletcher, F.J. Ahlers, A. Hartland, T.J.B.M. Janssen, IEEE T. Instrum. Meas. 52 (2003) 594–598.
[105] N.E. Fletcher, et al., Phys. Rev. B 68 (2003) 245310.
[106] N.E. Fletcher, T.J.B.M. Janssen, A. Hartland, in: Proceedings of BEMC'2001, Harrogate, 2001, IEE special issue, 2002.
[107] N. Feltin, L. Devoille, F. Piquemal, Bull. BNM, in press.
[108] M.W. Keller, A.L. Eichenberger, J.M. Martinis, N.M. Zimmerman, Science 285 (1999) 1706–1709.